Barrales Guadarrama, R.; Mocholí Salcedo, A.; Rodríguez Rodríguez, M.; Barrales Guadarrame, VR.; Vázquez Cerón, ER. (2013). A new forward-scatter visibility sensor based on a universal frequency-to-digital converter. Instrumentation Science and Technology. 41:445-462. doi:10.1080/10739149.2013.780250.

A New Forward-Scatter Visibility Sensor Based on a Universal Frequency-to-Digital Converter

R. Barrales-Guadarrama[1], A. Mocholí-Salcedo[2], M. E. Rodríguez-Rodríguez[1], V. R. Barrales-Guadarrama[1], E. R. Vázquez-Cerón[1]

[1]Área de Sensores y Procesamiento de Señales, Departamento de Electrónica, Universidad Autónoma Metropolitana—Azcapotzalco, México, D. F., México, [2]Grupo de Sistemas de Control de Tráfico, Departamento de Ingeniería Electrónica, Universidad Politécnica de Valencia, Valencia, España

Raymundo Barrales-Guadarrama Universidad Autónoma Metropolitana—Azcapotzalco, Departamento de Electrónica, Área de Sensores y Procesamiento de Señales, Av. San Pablo No. 180, Edif. H, Ofna. H-283, Col. Reynosa-Tamaulipas, México, D. F. 02200, México, Tel.: (55) 5318-9051, Ext. 1009; E-mail: rbg@correo.azc.uam.mx

Abstract

Traffic delays attributable to weather conditions may cause an increase in fuel consumption and then an increase in CO_2 emissions to the environment. Visibility reduction in roads due to dense fog is a main cause of traffic accidents and possible environmental pollution, hence the importance of deploying fog warning systems. In this paper, we present a forward-scatter visibility sensor that uses a quasi-digital photodetector and a universal frequency-to-digital converter instead of a conventional analog-to-digital converter as data acquisition system. This feature has allowed the design of a low cost, robust and simple sensor-to-microcontroller interface as demanded by Intelligent Transportation Systems (ITS) applications. An optical system to limit light interference is proposed. The visibilimeter was calibrated from a self-calibrated transmissometer using the same frequency-to-digital technique. This new instrument is capable of a 41 to 662.5 m visibility range detection and to transmit the information wirelessly to a 100 m distance.

KEYWORDS: Visibility, traffic control, energy saving, frequency-to-digital conversion

INTRODUCTION

Car accidents caused by fog and extreme weather are among the worst motorway accidents caused by meteorological conditions. Fog formation occurs when low temperatures over the road surface favour continuos water vapor condensation. Accidents arise when fog density causes a remarkable visibility reduction (less than 40 m)[1]. The severity of the accidents has driven some government departments to implement automatic prevention systems in roads where fog is a traditional problem. For example, in 2009, the California Department of Transportation and the California Highway Patrol started a 'Fog Pilot' project, an awareness fog and reduced-speed warning system that will help protect motorists along a 20 km stretch of freeway on State Route 99 in California's Central Valley. This particular stretch of freeway is notorious for dangerous fog conditions and was the site of a deadly 86-car collision in November 2007. Among other technologies, the 'Fog Pilot' includes visibility sensors. The warnings are communicated to drivers, in less than 30 seconds, via the large changeable message signs, which are placed every half mile[2]. Therefore, the main purpose in deploying visibility sensors along the roads is to prevent traffic accidents due to a dense fog, but these same instruments may contribute to saving energy and thereby reducing CO2 emissions[3]. Researchers at the Laboratory of Energy and the Environment at the Massachusetts Institute of Technology (MIT) reported that approximately 7 % energy of a vehicle is lost due to braking[4]. Hence, reducing braking may be assumed as a direct fuel savings

strategy. On the other hand, a car crash due to a dense fog imposes idling on the vehicles that follow the accident, a condition that has been identified to waste fuel[5]. Hence, abrupt acceleration and deceleration, braking and idling are vehicle operations that may occur during a fog event with consequences as energy waste and CO_2 emissions. Therefore, visibilimeters along with collision warning systems operating in a road segment where fog is a cause of accidents, may also help to reduce CO_2 emissions, contributing to a better environment.

Weather monitoring instruments used in ITS applications for preventing accidents need to be small, easy to put in operation on multiple measure sites, which implies low cost. The design and construction of ITS visibility sensors must fulfill specific goals according to these considerations. In this paper, we present a forward-scatter visibility sensor designed to measure a short visibility range of 41 to 662.5 m. Besides, a frequency-to-digital conversion technique was introduced in order to make a simplified sensor-to-microcontroller interface and cut costs. These two main features adapt the sensor to a regional ITS.

THE FORWARD-SCATTER MEASUREMENT PRINCIPLE

Several factors make visibility difficult to measure. Weather, sun angle, light intensity, dark adaptation, availability of appropriate visibility targets and individual physical abilities are all factors impacting observers in perceiving conditions in the atmosphere[6]. A standard was adopted to reduce visibility measurement difficulties. The standard quantity related to visibility is the Meteorological Optical Range (MOR). MOR is defined

by the World Meteorological Organization (WMO) as: "The lenght of path through the atmosphere required to reduce the luminous flux in a collimated beam from an incandescent lamp, at a colour temperature of 2700 K, to 0.05 of its original value, the luminous flux being evaluated by means of the photopic luminosity function of the International Commision on Illumination"[7]. When fog is present, visibility sensors determine MOR by measuring the local extinction coefficient, a parameter proportional to the reduction of the luminous flux, which is assumed to be constant around the sensor. This measurement is used to compute an equivalent observer´s visibility index. In the mid-to-late 70's, researchers began investigating the principle of "forward-scatter" for the measurement of the extinction coefficient, hence the visibility. Few papers report technological results[8,9]. The visibility is determined by the extinction coefficient σ defined by:

$$\frac{\partial E}{\partial l} = -\sigma E \qquad (1)$$

where E is the intensity of the light at position l. Solving (1), the fraction of light transmitted at lenght l from the light source is given by:

$$E(l)/E(0) = e^{-\sigma l} \qquad (2)$$

The lenght at which the light intensity is reduced to 5% can then be found:

$$MOR = 2.996/\sigma \, . \qquad (3)$$

Equation (3) is also known as the Koschmieder's Law (1925). Visibility can be measured by using optical scatter instruments. Figure 1 illustrates the basic principle.

An emitter sends a beam light and the scattered light intensity within the θ angle is received by the detector. A high signal output in the detector corresponds to a high

scattered intensity and a low visibility is measured. Different studies have been carried out to estimate visibility from the scattered intensity of light[10–13]. When $\theta \leq 90^{\circ}$, the instrument is known as a forward-scattering instrument. Commercial forward-scattering visibility sensors in ITS environments use IR LEDs as light sources. Some studies have theoretically reported the relationship between the extinction coefficient σ and the scattered intensity $E(\theta)$. It has been demonstrated[8,14] that the extinction coefficient depends on the particle size distribution modeling a fog sample and the scattering angle, but for a range $\theta \in [30^{\circ},40^{\circ}]$ [8] or $\theta \in [20^{\circ},50^{\circ}]$ [14], this dependence is minimal and σ is almost proportional to $E(\theta)$. A high lineal correlation between σ and $E(\theta)$ is observed for the angle $\theta = 35^{\circ}$ [8] or $\theta = 40^{\circ}$ [14]. Therefore, for a convenient θ range, the following relationship is valid:

$$\sigma = aE(\theta). \quad (4)$$

The PVM instrument[8] and the MIRA instrument[14] use this measurement principle. Both instruments use an IR LED as light transmitter. Visibility is then estimated applying (3).

INSTRUMENT IMPLEMENTATION

The proposed instrument is driven by the need to develop a visibility measurement system that relies on low cost commercially available hardware to simplify the sensor-to-control interface. Besides, the instrument is specified to be used for ITS applications which demand wireless communication capabilities for easy installation. It is important to note that hardware simplification was done by means of a universal frequency-to-digital

converter and this approach led to design compromises in the different instrument stages. Figure 2 shows the system block diagram.

The light source of the visibility sensor is a GaAs IR LED (SFH4508, OSRAM Optosemiconductors, Germany) with a total 40 mW radiant flux, emitting light at a 950 nm peak wavelength. As the distance from the lens tip IR LED to the detector is not specified in the radiation pattern curve, a 25 mm diameter plano-convex lens was added as a collimated light lens in order to restrict the radiated fog sample. In order to preserve a low junction temperature and high output intensity, the forward current was adjusted to be smaller than the maximum safe continuous value specified in the datasheet (100 mA). Good stable polarization is obtained by means of a low current adjustable positive regulator. As the sensor-to-microcontroller interface is a frequency-to-digital converter, a frequency output sensor was used. We chose a light-to-frequency converter (TSL245R, ams, Austria) combining a silicon photodiode and a current-to-frequency converter on single monolithic CMOS integrated circuit. The irradiance range detected by the sensor is 0.001 to 1000 $\mu W/cm^2$ with a 940 nm peak response. This detector is manufactured with an integral visible-light cutoff filter and lens. Figure 3 shows the final optical system design.

The quasi-digital photodetector used in this application generates a 50% duty cycle pulse train with frequency directly proportional to light intensity or irradiance. Frequency, as an informative parameter, has many advantages: high noise immunity, high output signal power, wide dynamic range, high accuracy of frequency standards, simplicity of signal

switching, interfacing, integration and coding. Therefore the dynamic range of the signal is not limited by supply voltage and noise, as it occurs with systems using analog-to-digital coverters (ADCs). Frequency-to-digital converters are capable of high accuracies up to 0.001%. In traditional measuring systems, ADC error is commensurable with the sensor's error[16,17]. Being a pulse data, the signals of several sensors may be easily multiplexed into one microcontroller. No output standardization for the ADC is necessary as in the case of analog sensors.

Different methods have been designed[16], in order to implement the frequency-to-digital conversion. Microcontrollers offer natural means for implementing such methods, but these devices require the use of program-oriented conversion methods. These introduce additional error components due to the so-called program-dependent or software related effects; for example, the error due to the delay of reaction to an interruption[18] and the error or shift in time of the response for interruption[19]. All these methods are unable to provide accurate, fast and wide range frequency measurements at the same time when they are programmed into a microcontroller. Actually, the methods of the dependent count are the best methods to implement the frequency-to-digital conversion. These methods combine the advantages of the classical methods as well as the methods ensuring constant relative error in a broad frequency range and high speed[20]. Taking into account the very wide output frequency range (0.001 kHz to 1000 kHz) of the light-to-frequency converter used in this project, the UFDC-1[21] (Sensors Web Portal, Canada) universal frequency-to-digital converter based on the methods of dependent count was used to implement the sensor-to-microcontroller interface. Minimum frequency accuracy

(1%) was programmed on the UFDC-1 and decimal numbers ommited from the registers. An SPI bus is the natural communication link between the UFDC-1 and the microcontroller (ATmega162, ATMEL, USA).

The instrument is not intended to be used as part of a monitoring network in the near future. It is rather to be used as a monitoring instrument wirelessly linked to a large changeable message sign placed along the road. Besides, data monitoring, among other test operations, is made on a regular PC that comes equiped with a Bluetooth wireless link. Because of these considerations and relative integration simplicity, a OEM Class 1 v2.0 + EDR Bluetooth-serial module (Parani ESD-1000, SENA, Korea) with a standard 100 m wireless transmit distance, was added to enable wireless communication capability. Figure 4 shows the circuit diagram of the main electronic system that allows visibility estimation. System integration meets the dimensions and cost requirements of an ITS device.

Ambient Light Interference Suppression

Generally, light signals and ambient light interference are deterministically located in the frequency domain and their electrical representations are present at the output of a transimpedance amplifier in photodetection systems. Such signals are relatively easy to separate when they are processed with a first or second order filter. This is not our case. The characteristic transfer function of the quasi-digital photodetector is[22]:

$$f = kE + f_D \quad (5)$$

where f is the output frequency of the sensor, k is the sensor responsivity, E is the irradiance and f_D is the sensor dark frequency. Tipically, f_D is very small (0.4 Hz) and can be neglected. Therefore, (5) is rewritten as:

$$f \approx kE . \qquad (6)$$

The output frequency vs. irradiance curve reported by the photodetector manufacturer[22] is obtained for a particular wavelength $\lambda_P = 940$ nm. It is clear that, when the photodetector is exposed to ambient light, it will generate a particular frequency signal proportional to the irradiance magnitude and the wavelength magnitude present at the moment:

$$\begin{aligned} f_{\lambda_0} &= k_0 E \\ f_{\lambda_1} &= k_1 E \\ f_{\lambda_2} &= k_2 E \\ &\bullet \\ &\bullet \\ &\bullet \\ f_{940} &= k_{940} E \\ &\bullet \\ &\bullet \\ f_{950} &= k_{950} E_S \\ &\bullet \\ &\bullet \end{aligned} \qquad (7)$$

The irradiance signal of interest is E_S which is produced by the IR LED at 950 nm. This irradiance must be filtered from the light spectrum received by the photodetector, in order to be further processed by the instrument and obtain the visibility magnitude. The necessary characterization of the optical system in Figure 3 has been reported elsewhere[23]. The important results obtained from this characterization are: (a) the experimental output frequency response as function of the incident irradiance for

different wavelengths in the interval 800 nm to 1100 nm, for the selected quasi-digital photodetector, Figure 5, that confirms the sensor's output frequency dependence upon the input wavelength; (b) the experimental relative responsivity as function of the wavelength, for the same sensor, Figure 6, where the peak response is located at 920 nm and the normalized response at 950 nm is 0.9; and (c) the sensor's response when it is provided with a bandpass interference filter (BIF) with a central wavelength at 950 nm, and a bandwidth of 10 nm[24], Figure 7. Practically, the study in Figure 7 demonstrates that the only irradiance detected is E_S at 950 nm from the IR LED. Once the BIF is added to the optical system of the visibility sensor, the instrument characterization may be carried on.

EXPERIMENTAL SETUPS

Frequency Characteristic

Output frequency response is one of the key characteristics of the instrument in order to obtain reliable visibility measurements with enough accuracy. Therefore, an experimental setup allowing the analysis of the relation $f_{OUT} = g(f_0)$, where f_{OUT} is the frequency measured by the UFDC-1 and f_0 is an input reference frequency, was designed. The experimental setup used to assess the output frequency response of the instrument is shown on Figure 8.

A TTL square wave of frequency f_0 was generated by a HP 33120A function generator as test signal for the instrument. The input reference frequency was measured with an

ESCORT EGC-3230 frequency counter. The output frequency, measured by the UFDC-1, was wirelessly transmitted to a computer and displayed in a virtual terminal.

Experimental Photodetector Responsivity

Experimental photodetector responsivity value must be taken into account in the signal processing program that allows the ambient light interference suppression. As shown in Figure 5, photodetector responsivity depends on the wavelength used and must be experimentally obtained since we work with a 950 nm wavelength and not the 920 nm peak detector response. Figure 9 shows the setup to obtain this parameter.

The IR LED intensity control provides a variable beam whose irradiance E is measured by the Newport 1835-C optical meter. The proportional frequency associated to this value and generated by the quasi-digital sensor is directly measured by the UFDC-1 in the instrument. The distance between the IR LED and the optical meter photodetector was chosen in a way to obtain high irradiance values, but to prevent photodetector saturation. The experiment was conducted under dark room conditions with the BIF as ambient light control measure.

EXPERIMENTAL RESULTS

Instrument Frequency Linearity

An ascending and descending data exploration, using the experimental setup of Figure 8, was done in order to apply a linear regression for the relation $f_{OUT} = g(f_0)$. Figure 10 shows the graphical result. The slope is m = 1.0041 Hz/Hz and the y intercept is b =

4.7123 Hz. These parameters were computed within the range [45 Hz, 800300 Hz], where the instrument sent valid lectures. The line defined by the equation $f_{OUT} = 1.0041 f_0 + 4.7123$ Hz is the best straight line from which the maximum non-linearity error in % FSS is (2608.6245/(800300-45))×100 ≈ 0.326%.

Photodetector Responsivity Measurement

A lineal regression upon the data obtained using the experimental setup in Figure 9 was performed in order to estimate the practical quasi-digital photodetector responsivity k. Figure 11 shows the experimental data distribution and the related adjusted curve when the experiment is conducted under laboratory conditions; in this case: k_1 = 0.036 kHz/μW/cm^2. Figure 11 also shows the result when the same experimental setup is used to obtain the quasi-digital sensor responsivity under field conditions (sunlight at 12:00 pm, sensor oriented to have the sun behind and the IR beam line oriented in the North line). In this case: k_2 = 0.04 kHz/μW/cm^2. Data analysis shows that relative error between the straight line slopes k_1 and k_2 is 10%. Responsivity $k = k_2$ was chosen to be 0.04 kHz/μW/cm^2 in the instrument.

CALIBRATION

As the BIF keeps a low relative error between the responsivity measured in laboratory and the responsivity measured in the field and non intense sunlight is present when ground fog appears because this type of fog is caused by the radiation cooling of the Earth's surface (radiation fog) which is caused after sunset, when the Earth receives no heat from the Sun[25], we decided to perform the calibration of the instrument under

laboratory conditions. If ambient light is reduced enough, the instrument can make an estimation of the extinction coefficient from (4):

$$\sigma = aE(40^{\circ}) = \frac{a}{k_2} f \,. \tag{8}$$

The Koschmieder's Law allows the instrument to estimate visibility from (3):

$$MOR = \frac{2.996}{\sigma} = \frac{2.996}{(a/k_2)f} \tag{9}$$

where k_2 is the sensor's responsivity and a is a constant that depends upon light beam intensity, the scattering geometry, and the detector sensitivity. The only practical method of determining the constant a is to compare the forward-scatter sensor's measurements to those from a transmissometer[26] or a standard visibilimeter. Due to the impossibilty of getting a visibilimeter or a transmissometer as standard instruments to proceed to a direct calibration process, an indirect calibration was conducted. Figure 12 shows the calibration setup of our own. A second quasi-digital sensor was added to the optical system of the visibilimeter in the θ = 0º direction, separated by a distance l = 300 mm from the light source emitting a constant irradiance E_0 in order to form a small transmissometer.

This setup was then placed in a Weiss Technik salt spray test chamber SC450 programmed to run a salt fog test (DIN ES ISO 9227) and frequency registers from the two sensors were taken once fog saturation was attained and the chamber deactivated. The chamber was isolated from ambient light. The average value of the frequency f_0 associated with the light source and the frequency generated by the transmissometer

sensor f_T are arranged in the Bouguer-Lambert Law to compute the extinction coefficient within the chamber:

$$\sigma_T = \frac{\ln\left[\frac{E_0}{E_l}\right]}{l} = \frac{\ln\left[\frac{f_0/k_2}{f_T/k_2}\right]}{l} = \frac{\ln[f_0/f_T]}{l}. \quad (10)$$

Assuming a homogeneous atmosphere, the visibilimeter extinction coefficient will be the same as for the small transmissometer. From (8):

$$\sigma_T = \sigma_V = aE_V(40^\circ) = a\frac{f_V(40^\circ)}{k_2}. \quad (11)$$

Frequency f_V measurements from the visibilimeter sensor generate indirect measurements of the irradiance E_V received by the instrument at $\theta = 40^\circ$ and frequency f_T measurements from the small transmissometer generate indirect measurements of the extinction coefficient σ_T. To obtain an estimation of *a*, a first order regression was performed for these indirect registers. Figure 13 shows the result for two register sets.

MEASUREMENT PROCEDURE

We used a CodeVisionAVR ver. 2.05.9 ANSI C compiler to program the microcontroller. Figure 14 shows the flow chart of the program. The basic steps of the system procedures are:

1. The quasi-digital sensor output frequency is firstly measured and processed by the UFDC-1. The configuration parameters for this device are sent from the microcontroller. The frequency measured is proportional to irradiance for θ = 40º and the final measurement is the result of averaging 10 consecutive frequency data.

2. The extinction coefficient σ_T is computed from the irradiance measured previously and a visibility (MOR) result is obtained.

3. The following visibility result is obtained once a 5 minute delay has passed. This prevents the instrument from monitoring visibility in a false fog condition.

The spray chamber allows a visibility sensor frequency range $f_V(40º)$ register from 1854 to 29788 Hz. For this range, we have a corresponding extinction coefficient range σ_V from 0.0045 to 0.0726 cm^{-1} where this figure has been computed using the relation:

$$\sigma_V = aE_V(40º) = a\left(\frac{f_V(40º)}{k_2}\right) = 9.9151\times10^{-5}\left(\frac{f_V(40º)}{40.65}\right)$$ according to the calibration process. Applying the Koschmieder's Law (3) to this range the response of the visibility sensor may be estimated. This result is shown in Figure 15.

Figure 16 shows the visibilimeter when calibration was performed with the spray test chamber.

CONCLUSIONS AND FUTURE WORK

Very good linearity was observed between the UFDC-1 input and output frequencies. The maximum non-linearity error in % FSS was 0.326%. Nevertheless, the claimed frequency measurement range, 0.001 kHz to 1000 kHz, was not enterily swept by the instrument. The lower frequency range limit is 45 Hz and this could be the result of an involuntary zero introduction generated by the lag low pass filter connected at the UFDC frequency input, recommended by the manufacturer. Fortunately, this condition does not have an impact on the visibilimeter response because the MOR lower limit detected occurred at 1854 Hz. Accurate visibility measurements in ITS applications are not

necessary because warning systems alert drivers before they reach a fog area and they would have sufficient time to reduce speed. Therefore, minimum frequency accuracy (1%) was programmed on the UFDC-1. A positive point with regard to the calibration procedure may be mentioned: the use of a small transmissometer to estimate extinction coefficient is valid because the transmissometer is self calibrating, according to the Bouguer-Lambert Law. The main instrument characteristics are a estimated visibility range of 41.24 to 662.5 m, good UFDC linearity, reduced size, telemetric operation within 100 m, and low cost. Although uncertainty is not meaningful, a comparison with a standard visibilty sensor must be done to stablish real uncertanty. Though the first measurement instruments using UFDCs are developed to monitor only one measurand with no inherent interferences, studies must be carried on to understand the differences of using an UFDC when inherent noise or other kind of interferences are present in the signal variation.

ACKNOWLEDGEMENTS

Authors would like to thank the Universidad Autónoma Metropolitana—Azcapotzalco and the Universidad Politécnica de Valencia for their support provided in this work.

REFERENCES

1. MacHutchon, K.R.; Ryan, A. Fog Detection and Warning, A Novel Aproach to Sensor Location. *Proc. IEEE AFRICON* **1999**, *1*, 43-50.

2. News Section, p. 8, (April-March 2009), ITS International Electronic Magazine, [Online]. Available: www.itsinternational.com.

3. Shladover, S.E. Challenges to Evaluation of CO_2 Impacts of Intelligent Transportation Systems. *IEEE FISTS*, Vienna, June 2011.

4. Bandivadekar, A.; Bodek, K.; Cheah, L.; Evans, C.; Groode, T.; Heywood, J.; Kasseris, E.; Kromer, M.; Weiss, M., On the Road in 2035: Reducing Transportation's Petroleum Consumption and GHG Emissions, Report No. LFEE 2008-05 RP, MIT Laboratory for Energy and the Environment, Cambridge, Massachusetts, 2008.

5. Schrank, D.; Lomax, T.; Turner, S. TTI's Urban Mobility Report 2010, 2010, [Online], Avalaible: http://tti.tamu.edu/publications/catalog/record/?id=36580.

6. Bradley, J.T.; Kraus, K.; Townshend, T. Federal Citing Criteria for Automated Surface Weather Observations, 7th Symp. On Meteorological Observations and Instrumentation, New Orleans, LA, 1991, 207-210.

7. Organización Meteorológica Mundial, Guía de Instrumentos y Métodos de Observación Meteorológicos, Ginebra, 1990.

8. Winstanley, J.V.; Adams, M.J. Point Visibility Meter: A Forward Scatter Instrument for the Measurement of Aerosol Extinction Coefficient. *Applied Optics*, **1975**, *14*(9).

9. Horner, J.L. Analog Visibility Computer. *Appl. Opt.* **1976**, *15*, 999-1002.

10. Twomey, S.; Howell, H.B. The Relative Merit of White and Monochromatic Light for the Determination of Visibility by Backscattering Measurements. *Applied Optics*, **1965**, *4*(4), 501-506.

11. Fenn, R.W. Correlation Between Atmospheric Backscattering and Meteorological Visual Range. *Applied Optics* **1966**, (2), 5.

12. Vogt, H. Visibility Measurement Using Backscattered Light. *Journal of the Atmospheric Sciences* **1968**, *25*, 912-918.

13. Maffione, R.A.; Dana, D.R. Instruments and Methods for Measuring the Backward-Scattering Coefficient of Ocean Waters. *Applied Optics*, **1997**, (36), 24.

14. Tjugum, S.A.; Vaagen, J.S.; Jakobsen, T.; Hamre, B. Use of Optical Scatter Sensors for Measurement of Visibility. *J. Environ. Monit.* **2005**, *7*, 608-611.

15. Nebuloni, R. Empirical Relationships between Extinction Coefficient and Visibility in Fog. *Applied Optics* **2005**, *44*(18), 3795-3804.

16. Kirianaki, N.V.; Yurish, S.Y.; Shpak, N.O.; Deynega, V.P. *Data Acquisition and Signal Processing for Smart Sensors*; John Wiley & Sons: Chichester, UK, 2002, 280 pp.

17. Hlupic, N.; Butorac, J.; Kresic, M. Improved Frequency Measurement by Means of DMM and Verification of its Specifications. *IEEE Trans. Instrum. Meas.* **2005**, *54*(5), 1957-1963.

18. Prokin, M. Double Buffered Wide-range Frequency Measurement Method for Digital Tachometers. *IEEE Trans. Instrum. Meas.* **1991**, *40*(3), 606-610.

19. Yurish, S.Y.; Reverter, F.; Pallàs Areny, R. Measurement Error Analysis and Uncertainty Reduction for Period and Time Interval-to-digital Converters Based on Microcontrollers. *Meas. Sci. Technol.* **2005**, *16*(8), 1660-1666.

20. Kirianaki, N.V.; Yurish, S.Y.; Shpack, N.O. Methods of Dependent Count for Frequency Measurements. *Measurement* **2001**, *29*, 31-50.

21. (2004), Universal Frequency-to-Digital Converter (UFDC-1), Specification and Application Note, [Online], Available: http://www.sensorsportal.com/DOWNLOADS/UFDC_1.pdf.

22. (2005) Infrared Light-to-Frequency Converter (TSL245R), Datasheet, [Online], Avalaible: http://www.taosinc.com/productdetail.aspx?product=46.

23. Barrales-Guadarrama, R.; Mocholí-Salcedo, A.; Vázquez-Cerón, E.R.; Rodríguez-Rodríguez, M.E.; Barrales-Guadarrama, V.R. A Technique for Adapting a Quasi-digital Photodetector to a Frequency-to-digital Converter, Proceedings 2012 IEEE Electronics, Robotics and Automotive Mechanics Conference, CERMA 2012, Cuernavaca, Morelos, México, Nov. 20-23, 2012.

24. (2011) 700 – 999 nm Bandpass Interference Filters, [Online], Available: http://www.edmundoptics.com/products/displayproduct.cfm?productid=3198&PageNum=6&Sort=displayOrder&Order=asc#products.

25. AeroGrapher's Mate, Module 05—Basic Meteorology, Chapter 5, Atmospheric Phenomena, Radiation Fog, [Online]. Available: http://www.tpub.com/content/aerographer/14312/css/14312_143.htm.

26. Burnham, D.C. *Fog, Snow, and Rain Calibrations for Forward-scatter Visibility Sensors, Scientific and Engineering Solutions*; Inc.: Orleans, MA, 1993.

Figure 1. The measurement principle in optical scatter instruments.

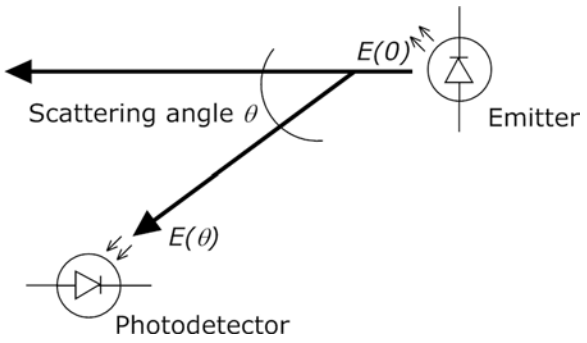

Figure 2. Visibility sensor block diagram.

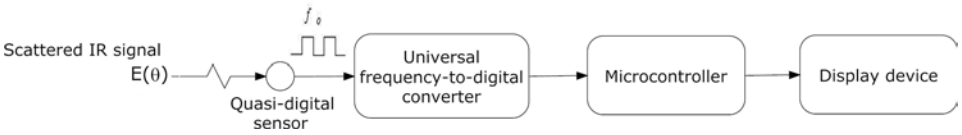

Figure 3. Mechanical drawing of the final optical sensor design. a. Quasi-digital sensor; b. Protective cover; c. 25 mm plano-convex lens; d. IR LED; e. Adjustable lens mount. Dimensions are in mm.

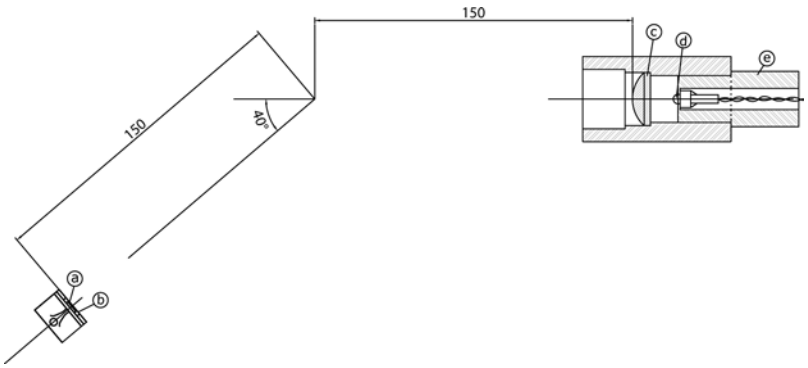

Figure 4. Complete circuit diagram of the visibilimeter instrument.

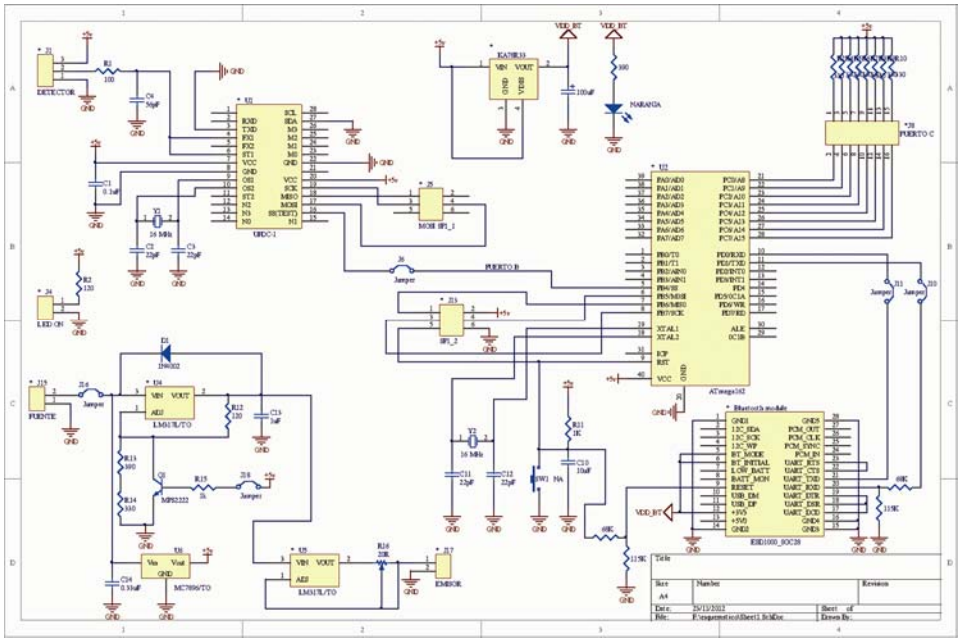

Figure 5. Experimental output frequency response as function of irradiance in TSL245R photodetector for different wavelengths.

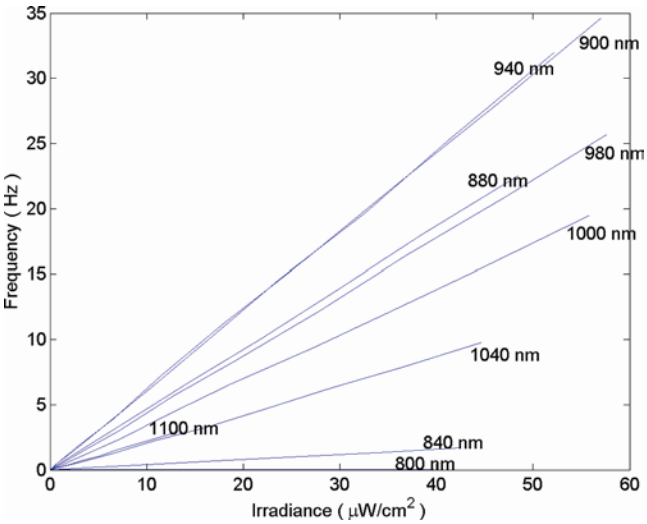

Figure 6. Experimental relative responsivity as function of the wavelength in TSL245R photodetector.

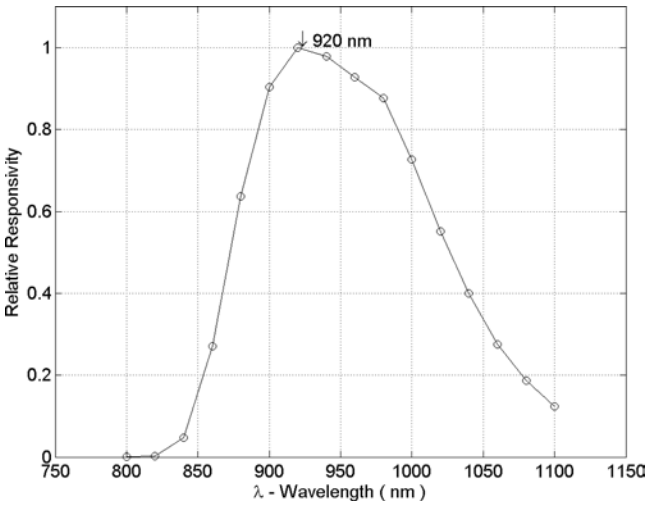

Figure 7. Experimental output frequency response as function of irradiance in TSL245R photodetector provided with a bandpass interference filter.

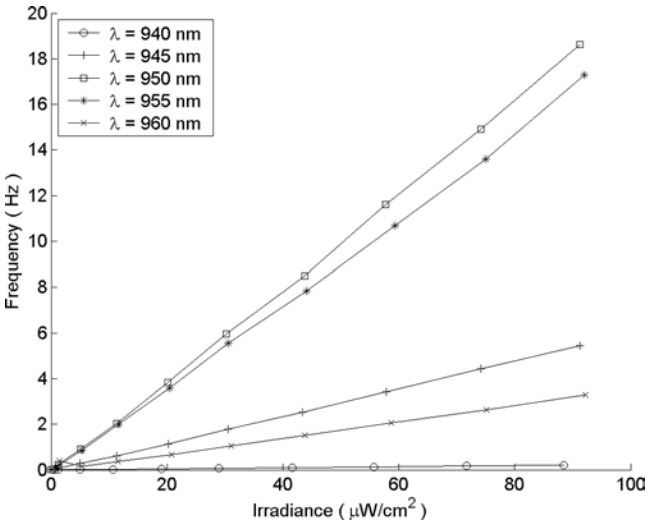

Figure 8. Experimental setup to assess the output frequency linearity.

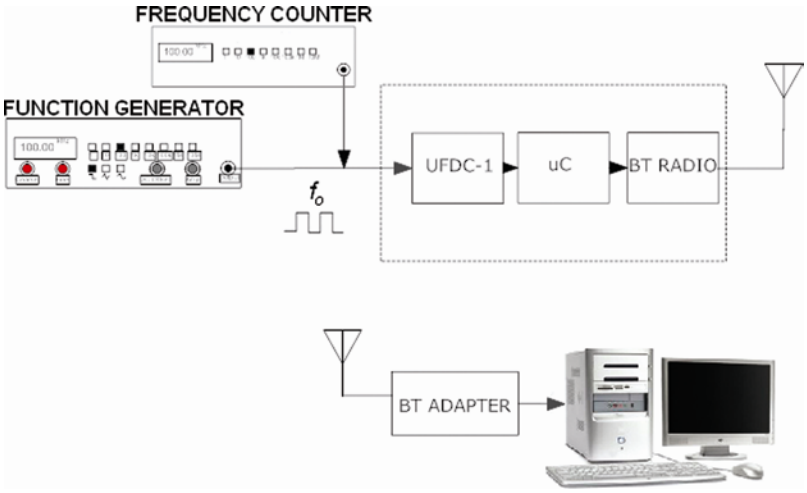

Figure 9. Experimental setup to measure the photodetector responsivity at λ = 950 nm.

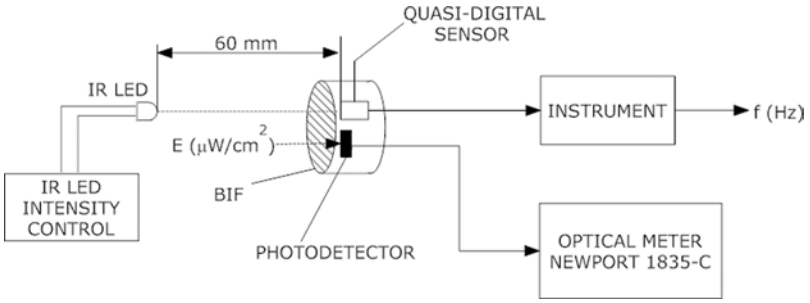

Figure 10. Frequency response of the instrument.

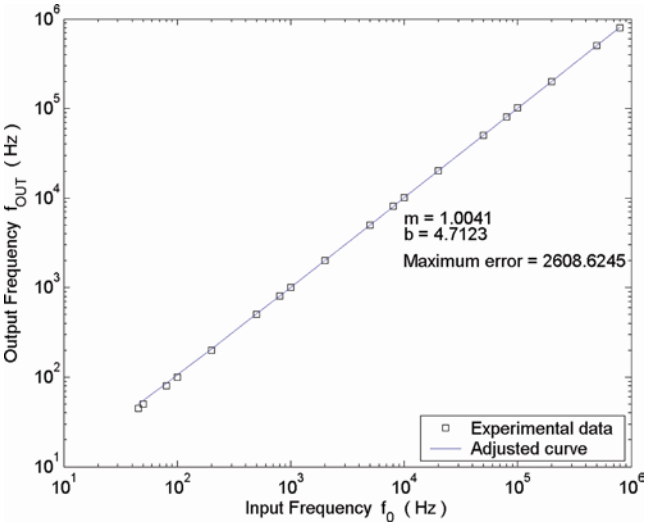

Figure 11. First order adjusted curve for the measurement of the sensor responsivity under laboratory conditions and field conditions.

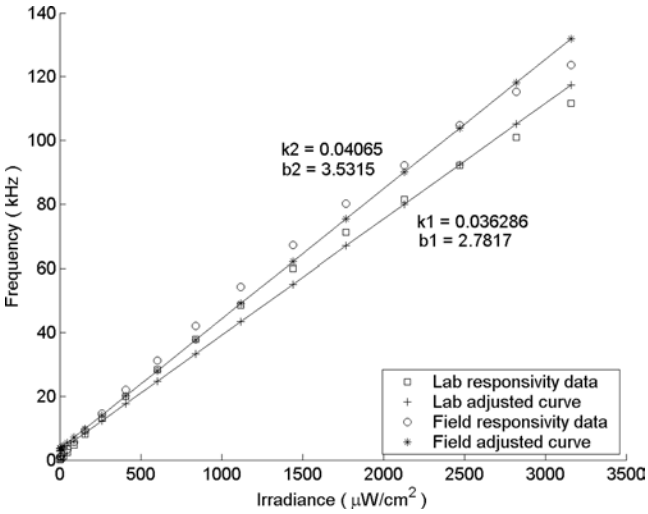

Figure 12. Mechanical drawing of the calibration setup.

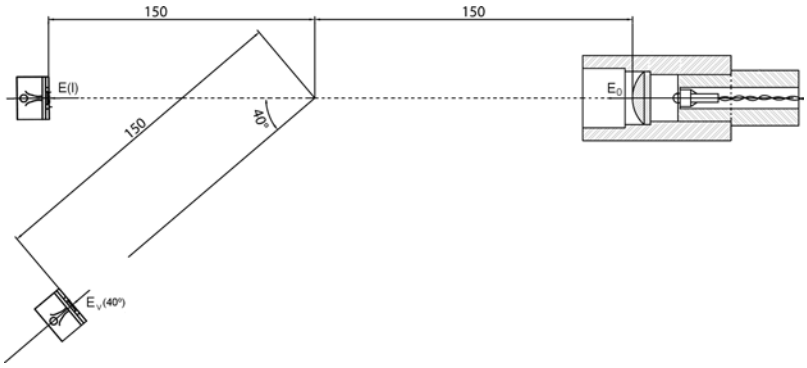

Figure 13. Estimation of *a* by first order regression.

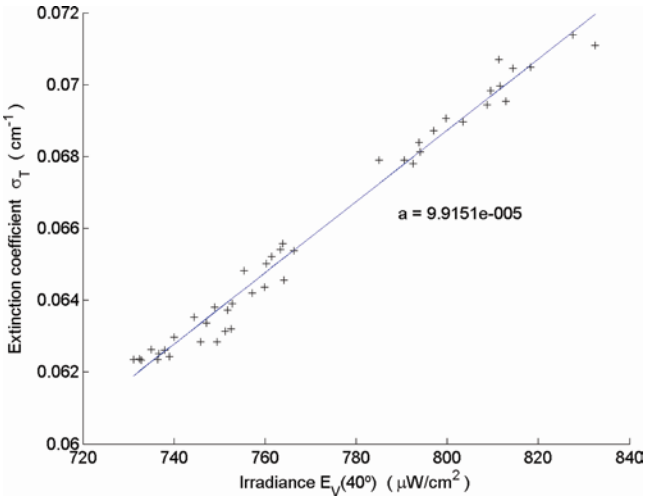

Figure 14. Flow chart of the measurement procedure.

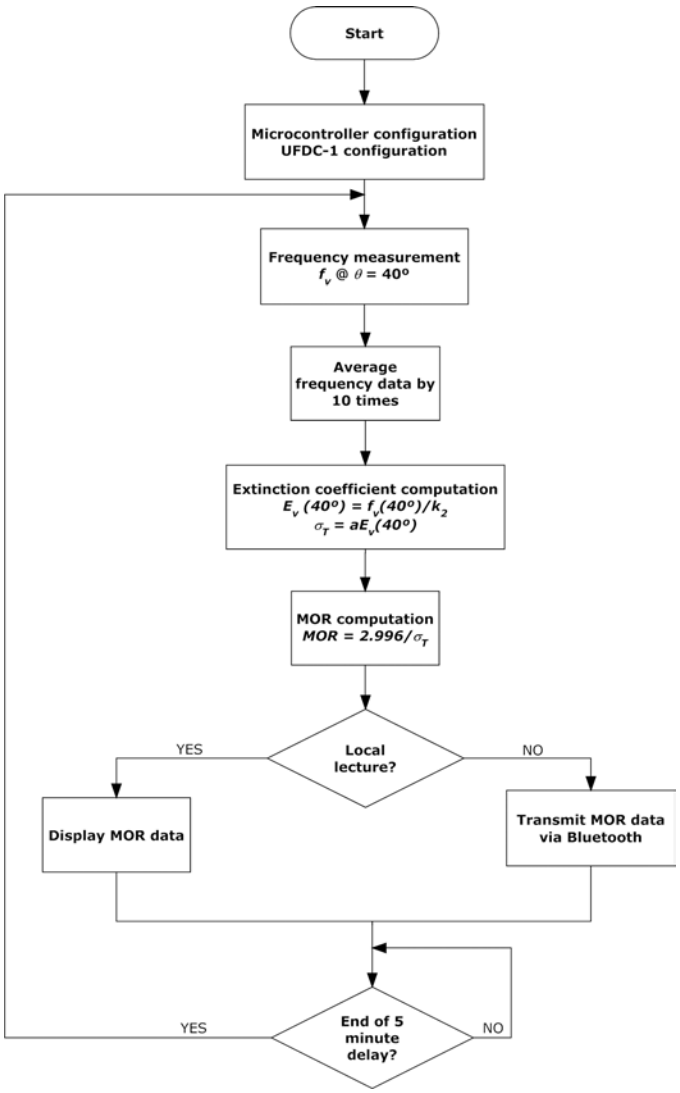

Figure 15. Estimated MOR response of the forward-scatter visibility sensor based on universal frequency-to-digital converter.

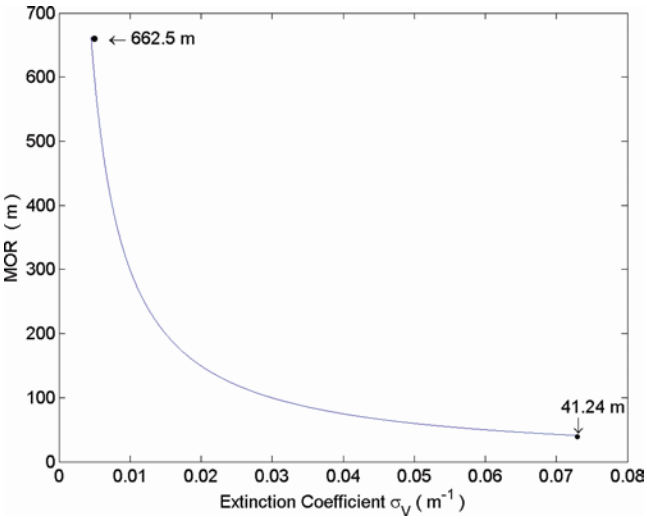

Figure 16. Photograph of the visibilimeter during calibration procedure.